# Temperature Dependent Elastic Constants (TDECs) and Thermodynamic Properties of B19 TiZr; Shape Memory Alloy (SMAs)

Job W. Wafula[1], George S. Manyali[2], John W. Makokha[1]

[1]*Department of Science, Technology and Engineering, Kibabii University, 1699-50200, Bungoma, Kenya,*
[2] *Computational and Theoretical Physics (CTheP), Department of Physical Sciences, Kaimosi Friends University College, 385-50309, Kaimosi, Kenya*

***Abstract:*** **We report temperature dependent elastic constants (TDECs) and thermodynamic properties of B19 TiZr Shape Memory Alloy (SMAs) computed by Quasi-static approximations (QSA) as implemented in thermo_pw code. B19 TiZr is mechanically and dynamically stable at zero pressure with lattice parameter of 3.110 Å and 1.578 for a and the ratio a/c respectively. The first-principles calculations were performed within quantum ESPRESSO code.**

***Key words*: Titanium Zirconium, elastic constants and thermodynamic properties**

## I. INTRODUCTION

Shape memory alloys (SMAs) undergo a transition from one phase to another when subjected to external stress or temperature change [1]. Temperature, pressure and atomic compositions determine the working of SMAs [2]. SMAs have several applications which include but not limited to surgery implants, actuators, dampers and in construction sectors incorporated into intelligent reinforced concrete [3]-[4]. The TiZr shape memory alloy has been reported as a high temperature shape memory alloy (HTSMA) thus attracted the interests of researchers [5]. Dental implants comprising TiZr shape memory alloys are better than pure Titanium due to high strength, especially for applications requiring small diameter implants [6]. The B19 phase of TiZr alloy is a hcp low temperature structure [7] of a space group P-6m2 (187). The TiZr SMA undergoes a reversible martensitic transformation from the hexagonal 'α' martensite to the cubic '$\beta$' austenite at the start temperature ($A_s$) of 871 K and the martensitic transformation with the start temperature ($M_s$) of 813 K [8]. Previous studies on B19 TiZr SMA have investigated the elastic properties mostly at zero pressure and temperature. Pressure dependent elastic constants of B19 TiZr were reported by Wang *et al* [9] however, temperature dependent elastic constants have not been investigated. In this paper, we computed temperature dependent elastic constants (TDECs) and thermodynamic properties of B19 TiZr SMA using Quasi-static approximation (QSA) implemented in thermo_pw code. The density functional theory (DFT) was used to solve the Kohn and Sham equation within the Quantum ESPRESSO code [10]. This paper is organized in the following sections; section 1; introduction, section 2; theory 3; the computational details are given. The results and discussion are presented in section 4. Finally, conclusion of our results is outlined in section 5.

## II. THEORY

Quasi-harmonic approximations (QHA) as implemented in thermo_pw code can be used to determine the temperature dependent elastic properties. QHA involve computing two parameters namely second derivative free energy with respect to strain and thermal expansion [11]. Helmholtz free energy at a constant temperature and volume of any structure of a material determined as follows;

$$F(V,T) = E_{static}(V) + F_{elec}(V,T) + F_{ph}(V,T) \quad (1)$$

$F_{ph}(V,T)$ is the phonon free energy, $F_{elec}(V,T)$ refers to the thermal free energy due to electronic excitations and $E_{static}(V)$ is static energy of the lattice at volume V and temperature T=0.

Static lattice energy and thermal free energy are computed by first principles static approach directly while QHA is used to evaluate phonon free energy as shown in equation (7).

$$F_{ph}(V,T) = \frac{1}{2}\sum_{qj}\hbar\omega_j(q,V) + k_BT\sum_{qj} ln\{1 - exp[-\hbar\omega_j(q,V)/k_BT]\} \quad (7)$$

$\omega_j(q,V)$ is phonon frequency of a $j^{th}$ mode of wave vector **q** in the first Brillouin zone (BZ), $\hbar$ is reduced Planks constant $(h/2\pi)$, and $k_B$ is Boltzmann constant.

QHA is computationally more expensive than Quasi-static approximation (QSA). QSA is a more simplified method of calculating temperature dependent elastic properties which assumes thermal dependence mostly on elastic moduli due to thermal expansion [11]. In Quasi-static approximations implemented in thermo_pw, temperature dependent elastic constants are computed in two steps procedure. The first step, static elastic constants at 0 K are calculated using stress-strain approach. Secondly, the calculated elastic constants in the first step at the volume *V (T, P)* are computed functions of temperature.

Temperature dependent elastic properties are computed by quasi-static approximations as follows; [12]

$$C_{ij}^{T}(T) = \frac{1}{V(T)} \frac{\partial^2 E}{\partial \eta_i \partial \eta_j}\Big|_{\eta=0} \quad (2)$$

V(T) is thermal expansion of the system determined from the quasi-harmonic approximation while second derivatives of energy with respect to strain are calculated using the static internal energy denoted E.

The Quasi-static approximation brings down cost of running computational calculations of temperature dependent elastic constants and always it considers the important fraction of thermal effects on elastic response of structures.

Adiabatic elastic constants are larger in most cases compared to their corresponding isothermal elastic constants as shown in the equation 3 [13].

$$C_{ij}^{s}(T) = C_{ij}^{T}(T) + \frac{TV\ {}_i\lambda_j}{C_v} \quad (3)$$

Where $C_V = (\partial E/\partial T)_V$ and $\lambda_i = -\sum_j \alpha_j C_{ij}^{T}(T)$.

Therefore, temperature dependent elastic constants for hcp symmetry are determined as follows; [14]

$$C_{44}^{s} = C_{44}^{T} \quad (4)$$

$$C_{11}^{s} = C_{11}^{T} + TV(\beta B_T)^2/C_V \quad (5)$$

$$C_{12}^{s} = C_{12}^{T} + TV(\beta B_T)^2/C_V \quad (6)$$

$$C_{13}^{s} = C_{13}^{T} + TV(\beta B_T)^2/C_V \quad (7)$$

$$C_{33}^{s} = C_{33}^{T} + TV(\beta B_T)^2/C_V \quad (8)$$

Where $B_T$ and $\beta$ are isothermal bulk modulus and volume thermal expansion coefficient computed by following equations

$$B_T = V(\frac{\partial^2 F}{\partial V^2})_T \quad (9)$$

$$\beta = (\frac{\partial V}{\partial T})_p/V \quad (10)$$

Adiabatic bulk modulus $B_S$ is calculated as follows;

$$B_s = \frac{B_T C_p}{C_V} = B_T + TV(\beta B_T)^2/C_V \quad (11)$$

Where $C_p$ is the isobaric heat capacity given by the following expression; [12]

$$C_p = C_V + VTB_T\beta^2 \quad (12)$$

In addition, from quasi-static approximations isothermal and adiabatic bulk moduli are computed as follows; [14]

$$B_T = \frac{C_{11}^{T}+2C_{12}^{T}}{3} \quad (13)$$

$$B_S = \frac{C_{11}^{S}+2C_{12}^{S}}{3} \quad (14)$$

## III. COMPUTATIONAL DETAILS

Temperature dependent elastic properties (TDECs) of α-TiZr shape memory alloy were computed by Quasi-static approximation (QSA) implemented in thermo_pw a post-processing code of Quantum ESPRESSO (QE). Projector augmented wave (PAW) [10] pseudo-potentials were applied with Perdew, Burke and Enzorhof (PBE) exchange-correlation functional of Generalized Gradient Approximations (GGA) [15]. The valence electron configurations for Ti and Zr are $3d^3 4s^1$ and $4d^3 5s^1$. The plane wave cut-off energy was set as 38.2 Ry since it was sufficient to converge the total energy of α-TiZr alloy. K-point meshes of 8×8×6 for the Brillouin zone was sampled based on Monkhorst-Pack scheme [16]. The dynamical matrices were determined on a 2×2×1 **q**-point grid interpolated on 192×192×192 **q**-point mesh.

## IV. RESULTS AND DISCUSSIONS

### *A. Phase transition*

Both pressure and temperature induced phase transitions were determined by comparing the Gibbs and Helmholtz free energies of B2 and B19 phases of the TiZr SMA. The pressure-induced transition was determined by analyzing Gibbs free energies (G) as a function of pressures at zero temperature as indicated in Fig. 1. On the other hand the phase transition temperature at zero pressure was arrived at by studying Helmholtz free energies (Ger) at different temperatures as indicated in Fig. 1. The temperature-induced phase transition from B19→B2 in TiZr SMA was in the range of 790 K and these values were lower than the experimental value 813K [8].

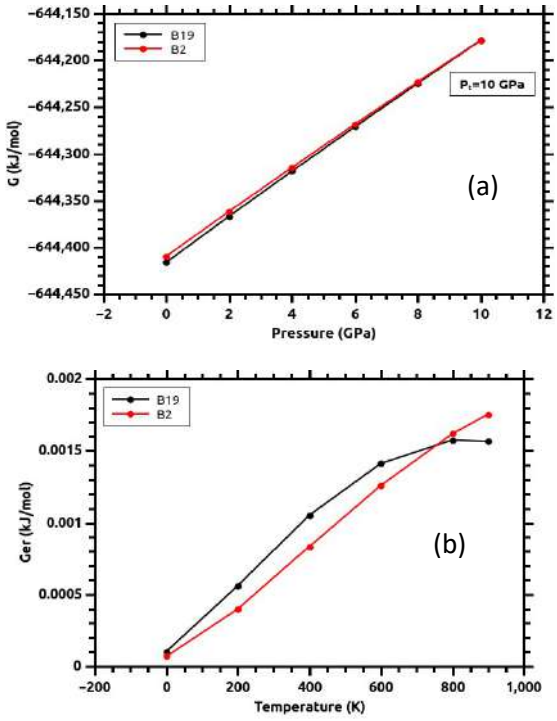


Fig. 1 (Colour online) Variation of (a) Gibbs and (b) Helmholtz free energy with temperature and pressure for hcp and cubic phases of TiZr alloy

*B. Structural properties*

Optimized geometry of B2 TiZr alloy was determined and atomic positions were relaxed at zero pressure and temperature. The energy versus volume data was computed and plotted as shown in Fig. 2. The equilibrium lattice constants were obtained by fitting the energy-volume data to the Birch-Murnghan equation of state (EOS) [16]. The plots of the total energy versus a and energy versus c/a are shown in Fig. 3 (a-b). The computed lattice constants of B2 TiZr alloy presented in table 1 are in good agreement with previous experimental and theoretical studies at 0 GPa and temperature thus the current study is consistency.

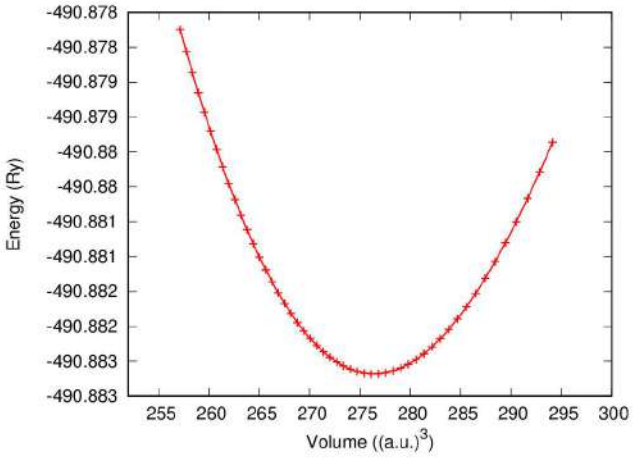


(a)

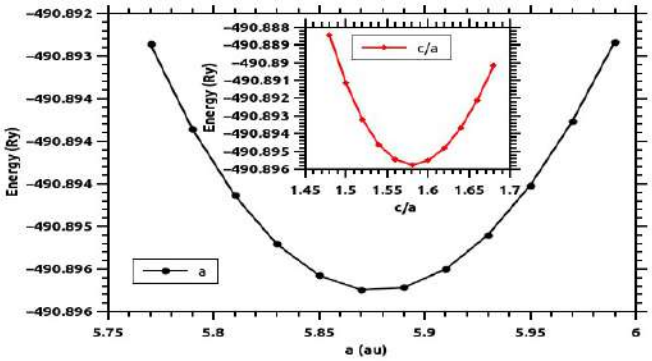


(b)

Fig. 2 (Colour online) (a) Energy versus volume plot and (b) energy versus a and c/a (inset) plots for hcp TiZr alloy

Table 1 Indicates equilibrium lattice parameters and elastic constants of hcp TiZr SMA in comparison with experimental and theoretical studies at zero pressure and temperature.

| B19 phase | a (Å) | c/a | $C_{11}$ | $C_{12}$ | $C_{13}$ | $C_{33}$ | $C_{44}$ |
|---|---|---|---|---|---|---|---|
| PBE-PAW | 3.110 | 1.578 | 159.8 | 55.5 | 68.9 | 169.5 | 31.0 |
| EXPT [17] | 3.104 | 1.586 | - | - | - | - | - |
| PBE-PAW [18] | 3.104 | 1.581 | 140.3 | 75.4 | 71.2 | 170.6 | 31.8 |
| PBE-PAW [9] | 3.111 | 1.579 | 145.1 | 72.5 | 70.9 | 169.0 | 30.0 |
| PBE-US [19] | 3.104 | - | 137.7 | 75.3 | 67.8 | 164.0 | 30.0 |

We also noted that the lattice constants of B19 TiZr SMA increase with temperature due to thermal expansion of the unit cell. For temperatures less than 100K, we observed small deviation in equilibrium lattice constant of α-TiZr SMA as indicated in Fig. 3 (a-b).

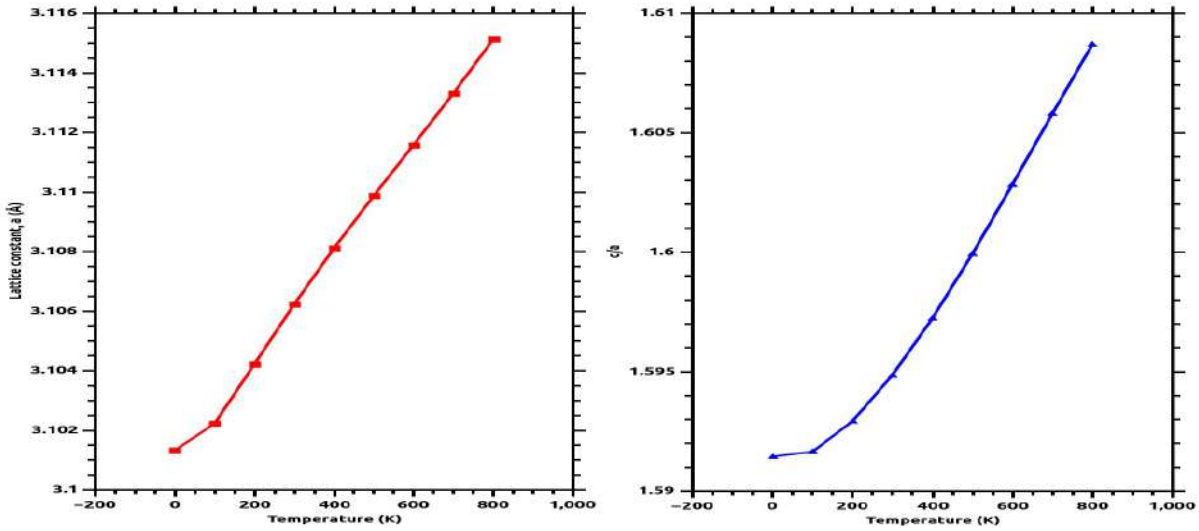


(a) (b)

Fig. 3 shows the variation of equilibrium lattice constants and the ratio c/aof the B19 TiZr SMA with temperature at zero pressure

### C. *Temperature dependent elastic constants (TDECs)*

Fig. 4 indicates the calculated temperature dependent elastic constants of B19 TiZr SMA. It is observed that elastic constants of the alloy decrease with increase in temperature because thermal expansion softens elastic constants as lattice vibration increases. Therefore, the ability of B19 TiZr SMA to resist against change in length and shape decreases with increase in temperature. The percentage softening of elastic constants was evaluated as follows; [20]

$$\frac{C_{ij}(T=0K)-C_{ij}(T=800)}{C_{ij}(T=0)} \times 100 \quad (15)$$

The obtained percentage softening of the isothermal elastic constants were as follows; 5%, 15%, 15%, 9% and 6% for $C_{11}$, $C_{12}$, $C_{13}$, $C_{33}$ and $C_{44}$. From Fig. 4 it is clear that adiabatic elastic constants (in red) are larger than the isothermal elastic constants (black) except elastic constant $C_{44}$ ($C_{44}^{S} = C_{44}^{T}$). Isothermal bulk modulus also decreases with temperature implying that the resistance against volume change declines at high temperatures as illustrated in Fig. 4.

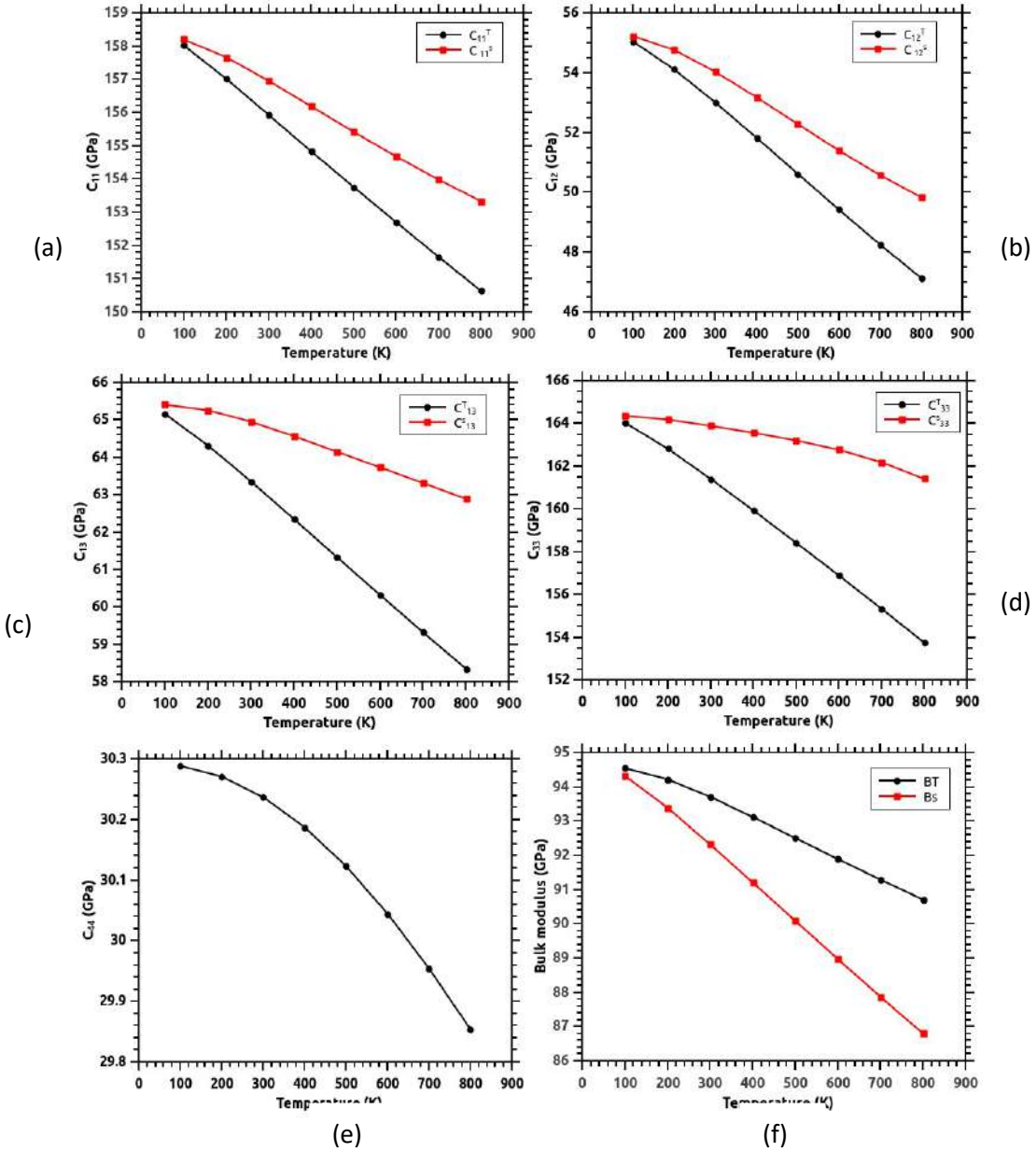


Fig. 4 shows (a-e) temperature dependent elastic constants $C_{ij}$ and (f) bulk modulus of B19 TiZr SMA at zero pressure.

*D. Thermodynamic properties*

Thermodynamic properties of the B2 TiZr alloy were calculated by the quasi-static approximation implemented in thermo_pw code within the temperature range of 0 K to 800 K. Phonon frequency of B2 TiZr SMA shown in Fig. 2 (e) indicates that the alloy is stable dynamically at zero pressure due to the absence of the imaginary phonons. The relationships between volume thermal expansion and temperature, Helmholtz free energy and temperature, Grùneisen parameter and temperature, volume and temperature are illustrated in Fig. 5 (a-e)

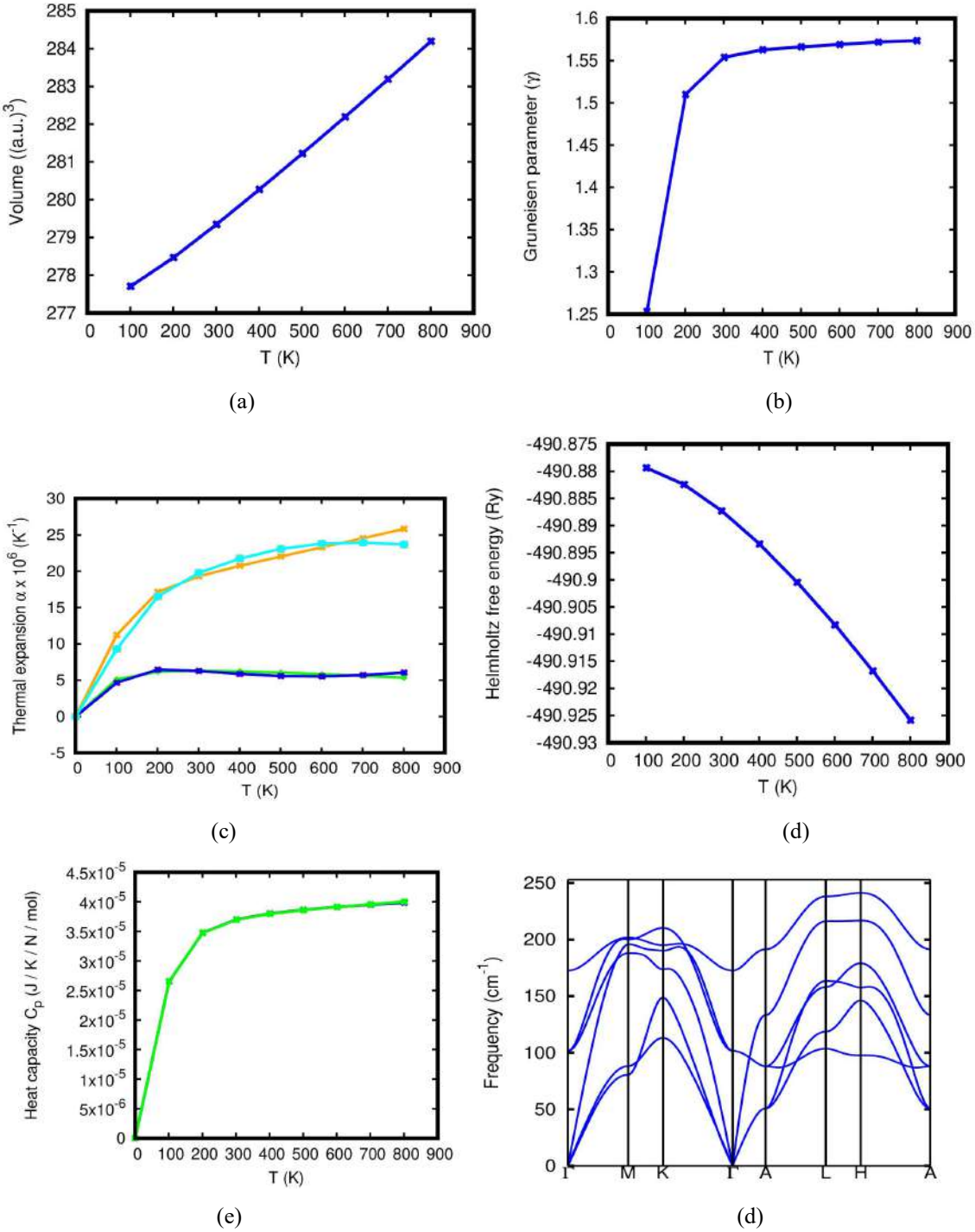


Fig. 5 Shows the variation of (a) volume, (b) Grùneisen parameter, (c) thermal expansion coefficient (blue/green represents vibrations in xx-directions whereas Orange/cyan in zz-directions), (d) Helmholtz free energy and (e) heat capacity at constant pressure Cp of the B19 TiZr alloy with temperature at 0 GPa pressure. (f) Indicates the phonon frequency of B19 TiZr alloy at zero pressure and temperature.

We observed that the volume B19 TiZr alloy has almost linear increase with the temperature however Helmholtz free energy decreases non-linearly as shown in Fig. 5 (a-b). Grùneisen parameter of B19 TiZr alloy increases rapidly below 300 K and gradually remains constant at higher temperatures as displayed in Fig. 5 (b). Specific heat capacity at constant pressure (Cp) is significant for better description of thermal properties [21]. Cp values of B19 TiZr alloy in Fig. 5 (e) increases steeply with increase in temperature and later remain constant at above 400 K temperature obeying the classical Dulong-petit law limit [22]. The coefficient of thermal expansion (α) is associated with the asymmetry of the thermal vibrations of the atoms [21]. It can be observed that α increase with increase in temperature at 0 GPa pressure illustrated in Fig. 2 (c). Vibrations along the zz direction are greater than in xx-direction.

## V. CONCLUSION

The lattice constants of the B19 TiZr SMA are in a reasonable agreement with experimental and theoretical studies at zero temperature. The B19 TiZr SMA is stable mechanically and thermodynamically at zero pressure and temperature. The elastic constants of B19 TiZr SMA decrease with increase in the temperature due to thermal expansion.

## ACKNOWLEDGEMENT

The authors thank the Department of Science, Technology and Engineering, Kibabii University, Kenya for providing the platform to carry out this research. Secondly, we acknowledge the Center for High Performance Computing (CHPC) based in South Africa for providing computational resources.

## REFERENCES

[1] Otsuka, K., & Ren, X. (1999). Recent developments in the research of shape memory alloys. Intermetallics, 7(5), 511-528.
[2] Rastogi, R., & Pawar, S. J. (2019). A computational study of shape memory effect and pseudoelasticity of NiTi alloy under uniaxial tension during complete and partial phase transformation. Materials Research Express, 6(5), 055702.
[3] Jani, J. M., Leary, M., Subic, A., & Gibson, M. A. (2014). A review of shape memory alloy research, applications and opportunities. Materials & Design (1980-2015), 56, 1078-1113.
[4] Chang, W. S., & Araki, Y. (2016, February). Use of shape-memory alloys in construction: a critical review. In Proceedings of the Institution of Civil Engineers-Civil Engineering (Vol. 169, No. 2, pp. 87-95). Thomas Telford Ltd.
[5] Baloyi, M. E., Modiba, R., Chauke, H. R., & Ngoepe, P. E. (2018). Computational study of binary titanium-based potential shape memory alloys. MS&E, 430(1), 012020.
[6] Kulkarni, M., Mazare, A., Schmuki, P., & Iglič, A. (2014). Biomaterial surface modification of titanium and titanium alloys for medical applications. Nanomedicine, 111, 111.
[7] Baker, H. (1992). Introduction to alloy phase diagrams. Materials Park, OH: ASM International, 1992. 1. 1.
[8] Li, Y., Cui, Y., Zhang, F., & Xu, H. (2011). Shape memory behavior in Ti–Zr alloys. Scripta Materialia, 64(6), 584-587.
[9] Wang, Y., Wang, J. J., Zhang, H., Manga, V. R., Shang, S. L., Chen, L. Q., & Liu, Z. K. (2010). A first-principles approach to finite temperature elastic constants. Journal of Physics: Condensed Matter, 22(22), 225404.
[10] Giannozzi, P., Baroni, S., Bonini, N., Calandra, M., Car, R., Cavazzoni, C., Ceresoli, D., Chiarotti, G., Cococcioni, G., Dabo, I., et al., (2017). Journal of Physics: Condensed Matter, 29, 465901.
[11] Destefanis, M., Ravoux, C., Cossard, A., & Erba, A. (2019). Thermo-elasticity of materials from quasi-harmonic calculations. Minerals, 9(1), 16.
[12] Wang, Y., & Li, L. (2000). Mean-field potential approach to thermodynamic properties of metal: Al as a prototype. Physical Review B, 62(1), 196.
[13] Davies, G. F. (1974). Effective elastic moduli under hydrostatic stress—I. quasi-harmonic theory. Journal of Physics and Chemistry of Solids, 35(11), 1513-1520.
[14] Gülseren, O., & Cohen, R. E. (2002). High-pressure thermoelasticity of body-centered-cubic tantalum. Physical Review B, 65(6), 064103.
[15] Perdew, J. P., Burke, K., & Ernzerhof, M. (1996). Generalized gradient approximation made simple. Physical review letters, 77(18), 3865.
[16] Murnaghan, F. D. (1944). The compressibility of media under extreme pressures. Proceedings of the national academy of sciences of the United States of America, 30(9), 244.
[17] Bashkin, I. O., Fedotov, V. K., Nefedova, M. V., Tissen, V. G., Ponyatovsky, E. G., Schiwek, A., & Holzapfel, W. B. (2003). Crystal structure and superconductivity of TiZr up to 57 GPa. Physical Review B, 68(5), 054401.
[18] Zhang, C. B., Li, W. D., Zhang, P., & Wang, B. T. (2020). Phase transition, elasticity, phonon spectra, and superconductive properties of equiatomic TiZr, TiHf, and ZrHf alloys at high pressure: Ab initio calculations. Computational Materials Science, 178, 109637.
[19] Ikehata, H., Nagasako, N., Furuta, T., Fukumoto, A., Miwa, K., & Saito, T. (2004). First-principles calculations for development of low elastic modulus Ti alloys. Physical Review B, 70(17), 174113.
[20] Malica, C., & Dal Corso, A. (2020). Temperature dependent elastic constants and thermodynamic properties of BAs: An ab initio investigation. Journal of Applied Physics, 127(24), 245103.
[21] Mebtouche, H., Baraka, O., Yakoubi, A., Khenata, R., Tahir, S. A., Ahmed, R., ... & Wang, X. (2020). First-principles calculations of the structural, electronic, mechanical and thermodynamic properties of MAX Phase Mon+ 1GeCn (n= 1, 2, and 3) compounds. Materials Today Communications, 101420.
[22] Petit, A. T., & Dulong, P. L. (1819). Study on the measurement of specific heat of solids. *Ann. Chim. Phys*, *10*, 395-413.